

Document downloaded from:

<http://hdl.handle.net/10251/166456>

This paper must be cited as:

Palumbo, F.; Andreu Ros, Ml.; Brunetti, M.; Schmallegger, M.; Gescheidt, G.; Neshchadin, D.; Miranda Alonso, MÀ. (2019). Hydrogen Abstraction from the C15 Position of the Cholesterol Skeleton. *The Journal of Organic Chemistry*. 84(23):15184-15191.
<https://doi.org/10.1021/acs.joc.9b02181>



The final publication is available at

<https://doi.org/10.1021/acs.joc.9b02181>

Copyright American Chemical Society

Additional Information

1 **Hydrogen abstraction from the C15 position of the cholesterol**
2 **skeleton**

3 Fabrizio Palumbo,^a Inmaculada Andreu,^{*a,c} Maria Brunetti,^a Max Schmallegger,^b Georg
4 Gescheidt,^b Dmytro Neshchadin,^{*b} and Miguel A. Miranda^{*a,c}

5

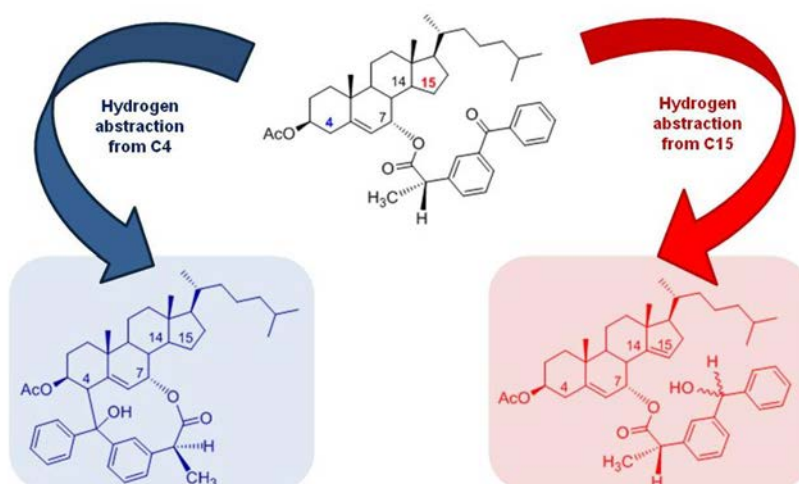
6 ^a Instituto de Tecnología Química UPV-CSIC, Universitat Politècnica de València, Camino
7 de Vera s/n, 46022 Valencia, Spain. E-mail: mmiranda@qim.upv.es

8 ^b Institute of Physical and Theoretical Chemistry, Graz University of Technology, NAWI
9 Graz, Stremayrgasse 9/I, 8010 Graz, Austria. E-mail: neshchadin@tugraz.at

10 ^c Unidad Mixta de Investigación UPV-Instituto de Investigación Sanitaria (IIS) La Fe,
11 Hospital Universitari i Politècnic La Fe, Avenida de Fernando Abril Martorell 106, 46026
12 Valencia, Spain. E-mail: iandreur@qim.upv.es

13

14 **Abstract graphic**



15

16 **Abstract**

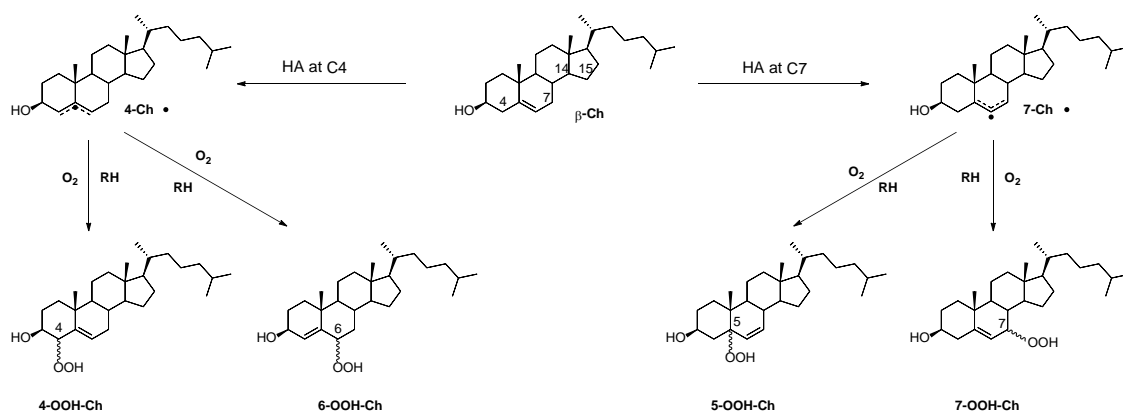
17 Cholesterol (**Ch**) is an integral part of cell membranes, where it is prone to oxidation. In
18 humans, oxidation of **Ch** is commonly linked to various pathologies like Alzheimer's,
19 atherosclerosis and even cancer, which proceed *via* mechanisms involving enzymatic
20 and free radical pathways. The latter begin with hydrogen abstraction (HA) from **Ch** by
21 a reactive free radical. It has been established that the most efficient HA from **Ch** occurs
22 at C7, although HA from C4 by peroxy radicals has recently been observed. Conversely,
23 HA from **Ch** positions other than the thermodynamically preferred C7 or C4 **has never**
24 **been reported**. We have designed a **Ch** derivative where a benzophenone moiety is
25 linked to C7 by a covalent bond. This mirrors a specific orientation of **Ch** within a
26 confined environment. Product analysis and time-resolved spectroscopic studies reveal
27 an unprecedented HA from C15, which is a thermodynamically unfavorable position.
28 This indicates that a specific topology of reactants is crucial for the reactivity of **Ch**. The
29 relative orientation of the reactants can also be relevant in biological membranes, where
30 **Ch**, polyunsaturated fatty acids (PUFA) and numerous oxidizing species are confined in
31 highly restricted and anisotropic environments.

32 **Introduction**

33 Cholesterol (**Ch**) is one of the most important building blocks of eukaryotic cells. This
34 molecule carries out multiple functions in cell membranes: it controls membrane fluidity
35 and permeability, composing rigid rafts to support various membrane proteins.
36 Moreover, **Ch** plays a significant role in the biosynthesis of numerous hormones, vitamin
37 D, and bile acids. Cholesterol is also one of the main targets for oxidation in cell

38 membranes. In humans, oxidation of **Ch** is commonly linked to various pathologies like
39 Alzheimer's, atherosclerosis and even cancer.¹⁻⁶ Such detrimental processes proceed *via*
40 distinct mechanisms, including enzymatic and free radical pathways. The latter begin
41 with hydrogen abstraction (HA) from **Ch** by a reactive free radical (Scheme 1) primarily
42 forming a **Ch**-derived radical.⁷ The follow-up reaction with molecular oxygen leads to
43 peroxy radicals that, in turn, can abstract hydrogen from another **Ch** molecule,
44 polyunsaturated fatty acids, or antioxidants.⁸ Oxidation *via* radicals *in vivo* may be
45 caused by reactive oxygen species but also various photo-sensitive drugs like ketoprofen
46 that are capable of abstracting hydrogen atoms from biological targets like
47 polyunsaturated fatty acids (PUFA) and DNA inducing potentially damaging chemical
48 reactions. Indeed, ketoprofen⁹ (2-(3-benzoylphenyl)propanoic acid), which is widely
49 used as non-steroidal anti-inflammatory drug (NSAID) with analgesic and antipyretic
50 effects, is able to absorb UVA light that can penetrate the middle layer of skin (the
51 dermis), inducing frequently phototoxic and photoallergic effects in patients.^{10,11}
52 The primary HA from a steroid skeleton by photoexcited benzophenone has been largely
53 investigated by Breslow and coworkers many years ago.^{12,13} They have synthesized
54 saturated dihydrosteroid derivatives (e.g. 3 α -cholestanol) comprising a benzophenone
55 moiety. Based on product analysis of irradiated solutions, CD spectra, phosphorescence
56 lifetime, and molecular models, they could show that HA is directed mainly by the
57 topology of the steroid/benzophenone dyads. In contrast to dihydrosteroids, **Ch** carries
58 a double bond at **C5-C6**. In this latter case, it is well established that the most efficient
59 hydrogen abstraction occurs from C7 and C4.¹⁴ Evidently, the bond dissociation energies
60 (BDE) of the allylic hydrogens, C7-H and C4-H are the lowest in the steroid core of **Ch**.
61 Therefore such a selectivity of hydrogen transfer can be explained by thermodynamic

62 control. However, in complex and inhomogeneous environments like membranes, even
 63 small molecules can be forced to a confined orientation.¹⁵ This may cause entropic
 64 factors to become dominant. Farez *et al.* detected 15 α -hydroxycholestene (15-HC) in
 65 patients with secondary progressive multiple sclerosis (SPMS).¹⁶ This 15-oxysterol can
 66 be, in principle, formed as a result of an initial HA from C15 of cholesterol in cell
 67 membranes. Although the findings of Farez *et al.* are under debate,¹⁷ it is important to
 68 find out whether a thermodynamically unfavorable HA from **Ch** can be overruled by
 69 topological confinement. In addition, taking into account that the steroidal skeleton, as
 70 well as C–H functionalization, have attracted the attention of synthetic chemists for
 71 decades, the present work is of considerable interest in the field of basic organic
 72 chemistry, since it is focused on selective activation of stronger C–H bonds in the
 73 presence of weaker ones.^{18,19}



80 **Scheme 1.** Free radical oxidation of Cholesterol

81 We have shown that HA by the photo-excited triplet state of ketoprofen from
 82 cholesterol's core is predominantly controlled by entropic factors like the spatial

83 arrangement of reactants rather than by thermodynamic properties.²⁰ The question is
84 whether topology is a decisive factor for the selectivity of HA reactions in steroids, and
85 in this context we have designed and synthesized derivatives **1** and **2**. In these model
86 systems, the benzophenone fragment serves as a selective, photo-triggered
87 intramolecular hydrogen-abstrating agent with the reaction at C7 being prevented by
88 steric strain and conformational restrictions. It is our aim to shed light onto the role of
89 topology/entropy for the selectivity of the HA reaction. In a first step, steady-state UV
90 irradiation and product analysis provides access to the photo-induced conversions. To
91 avoid artifacts caused by undesired follow-up reactions of steady-state photolysis, we
92 have applied time-resolved methodology for substantiating the photo induced reaction
93 (Figure 1). To this end, we have utilized Laser Flash Photolysis (LFP) and Time-Resolved
94 Chemically Induced Dynamic Nuclear Polarization (TR-CIDNP).

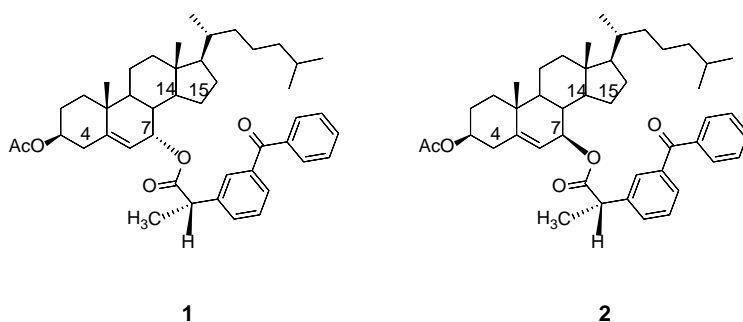


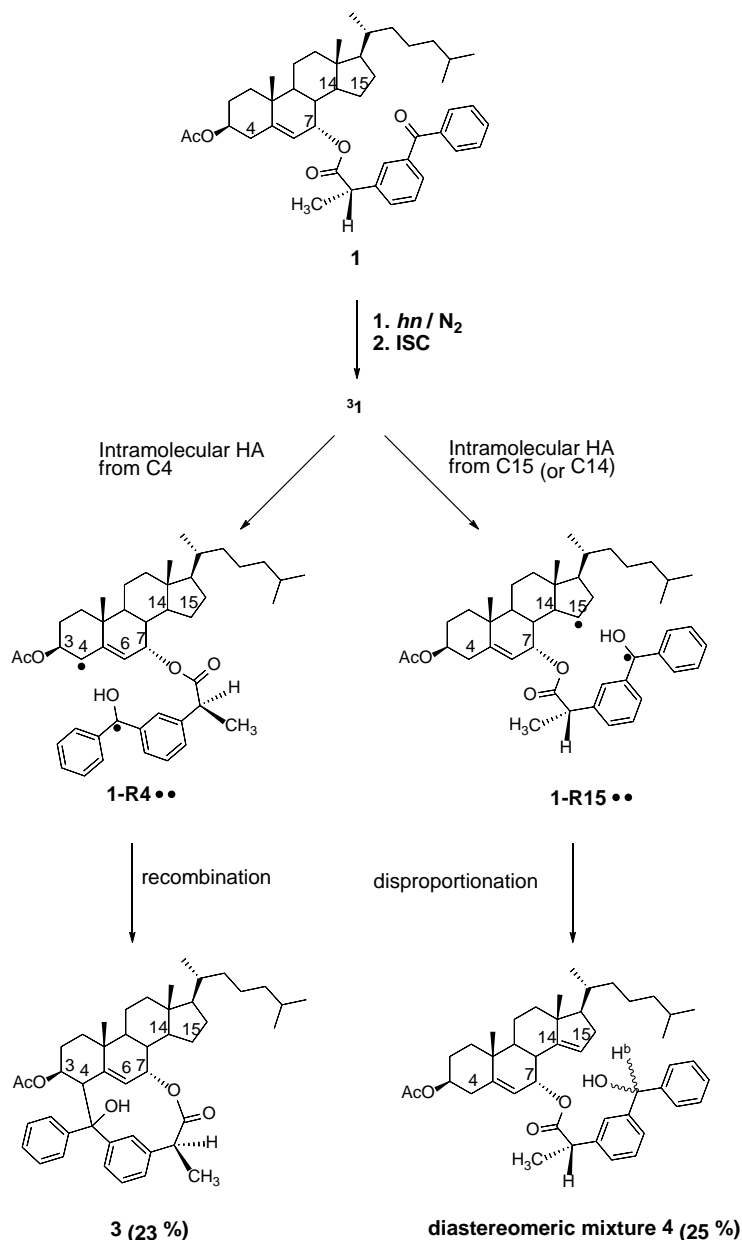
Figure 1 Chemical structures of diastereomeric dyads **1** and **2**

103 Results and discussion

104 We have arranged the presentation of our results in two separate sections, one
105 reporting on the photophysical/photochemical, the other on NMR/CIDNP-based
106 investigations supported with quantum mechanical calculations.

107 **Steady state irradiation and flash photolysis**

108 The diastereoisomeric esters **1** and **2** were prepared from acetylcholesterol (acetylCh)
109 and (S)- ketoprofen ((S)-KP) following standard procedures²¹ (see details in
110 Supplementary Information). Steady state irradiations of **1** and **2** were carried out in
111 dichloromethane solutions (*ca.* 3.5×10^{-3} M) under a nitrogen atmosphere, with a 400
112 W high-pressure mercury lamp as the light source. Even a long-term irradiation (8 hours)
113 of dyad **2** did not lead to any products. In contrast, dyad **1** reacted readily yielding
114 photoproducts **3** and **4** in similar quantities. Both **3** and **4** can only be formed *via*
115 intramolecular HA by the excited triplet state of the benzophenone moiety from carbons
116 C4 and C15 (or C14) of the steroid core. The overall photoreduction quantum yield for
117 dyad **1** was determined using a related compound (S)-KP-3 α -Ch as actinometer²² and its
118 value was found to be 0.43 (0.22 and 0.21 for the formation of photoproducts **3** and **4**,
119 respectively). Scheme 2 shows a likely reaction mechanism. Structural differences
120 between **1** and **2** that led to such a dissimilar reactivity will be discussed later.



121

122

Scheme 2 Intramolecular HA and follow-up products formation in dyad **1**

123 Photo-excitation of **1** leads to its triplet excited state, which is confined to the

124 benzophenone substituent and can abstract hydrogen atoms from the steroid fragment

125 of the molecule. Hydrogen abstraction from the position C4 of **1** results in biradical **1-**

126 **R4••**, subsequent recombination of the two radical centers in **1-R4••** yields

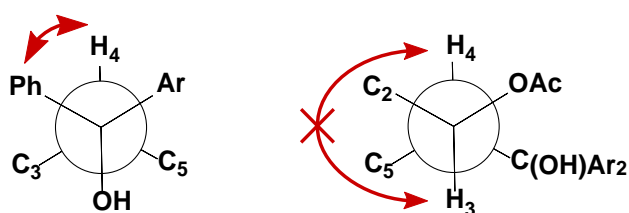
127 photoproduct **3**. On the other hand, HA from C15 (or C14) produces **4** via intramolecular

128 disproportionation of biradical **1-R15••** (or **1-R14••**). Remarkably, we did not observe

129 any disproportionation products after HA from C4, nor recombination products after HA
130 from C15 (C14).

131 We have established the structures of **3** and **4** unambiguously based on their NMR (^1H ,
132 ^{13}C , HSQC and NOESY) and mass spectra. In particular, NOESY experiments of
133 photoproduct **3** provided the stereochemistry of the new stereogenic center at C4
134 generated upon photocyclization. The most relevant interaction was found between the
135 allylic proton at C4 and the hydrogen atoms of the phenyl group. Moreover, it should be
136 noted that no NOE effect was found between the hydrogens at C4 and C3; this indicates
137 that both protons are in a trans configuration (Figure 2).

138



139

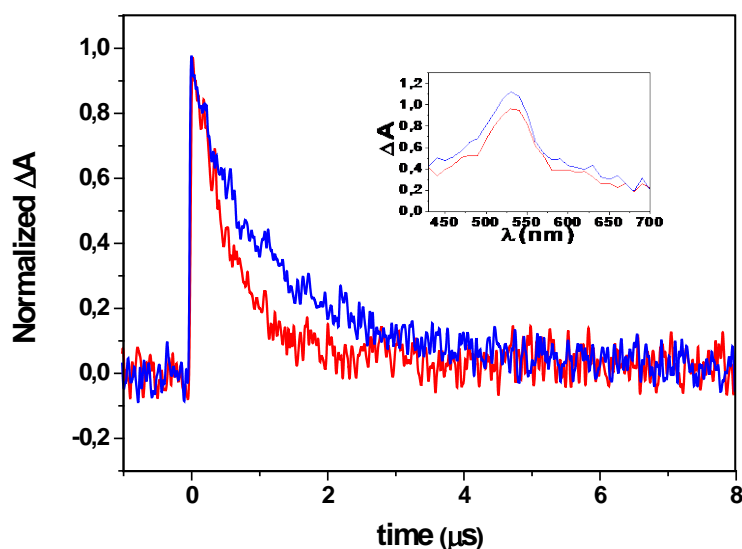
140

Figure 2. NOE interactions in **3**

141

142 To gain insight into the photochemical processes at a shorter time scale, dyads **1** and **2**
143 were probed by LFP ($\lambda_{\text{exc}} = 355 \text{ nm}$) in dichloromethane solutions, under an inert
144 atmosphere. The transient absorption spectrum of dyad **1**, obtained 0.3 μs after the
145 laser pulse (Figure 3), showed the exclusive presence of the benzophenone-based triplet
146 excited state with a characteristic maximum absorption at $\lambda_{\text{max}} = 525 \text{ nm}$. It was not
147 possible to detect biradicals **1-R4••** and **1-R15••** (or **1-R14••**) on the microsecond time
148 scale because their steady state concentrations are negligible due to rapid follow-up
149 reactions. This is borne out by the observation that for dyad **2**, which does not display
150 intramolecular follow-up reactions, the ketyl radical ($\lambda_{\text{max}} = 545 \text{ nm}$) was observed as a

151 result of a slow HA from the solvent, in addition to the triplet species. Kinetic analysis of
152 decay traces allowed determining the triplet lifetimes (τ_T) of **1** ($\tau_T = 0.60 \mu\text{s}$) and **2** ($\tau_T =$
153 $1.67 \mu\text{s}$). The latter matched the τ_T value of the reference **(S)-KP** in dichloromethane.¹⁹
154 The intramolecular quenching rate constant (i.e. the upper limit of the rate constant of
155 intramolecular HA) can be calculated using triplet lifetimes: $k_{iq} = 1/\tau_i - 1/\tau_0$, where τ_i and
156 τ_0 are triplet lifetimes of dyad and reference compound (**(S)-KP**, $\tau_0 = 1.6 \mu\text{s}$)
157 correspondingly. For dyad **1** the upper limit is $1.07 \times 10^6 \text{ s}^{-1}$ for either H atoms at C4 and
158 C15 (or C14). This strongly indicates that under UV irradiation **1** undergoes
159 intramolecular hydrogen abstraction that is in full agreement with the results of product
160 analysis after the longer irradiation times. The k_{iq} obtained for **1** was found to be one
161 order of magnitude lower than that determined for the intramolecular process in
162 compounds containing benzophenone and 1,4 cyclohexadienes as hydrogen donors.²³



163
164 **Figure 3.** Normalized transient decays for **1** (red) and **2** (blue) monitored at 620 nm in CH_2Cl_2 . Insert:
165 transient absorption of **1** and **2** (blue) recorded $0.3 \mu\text{s}$ after the laser flash.

166

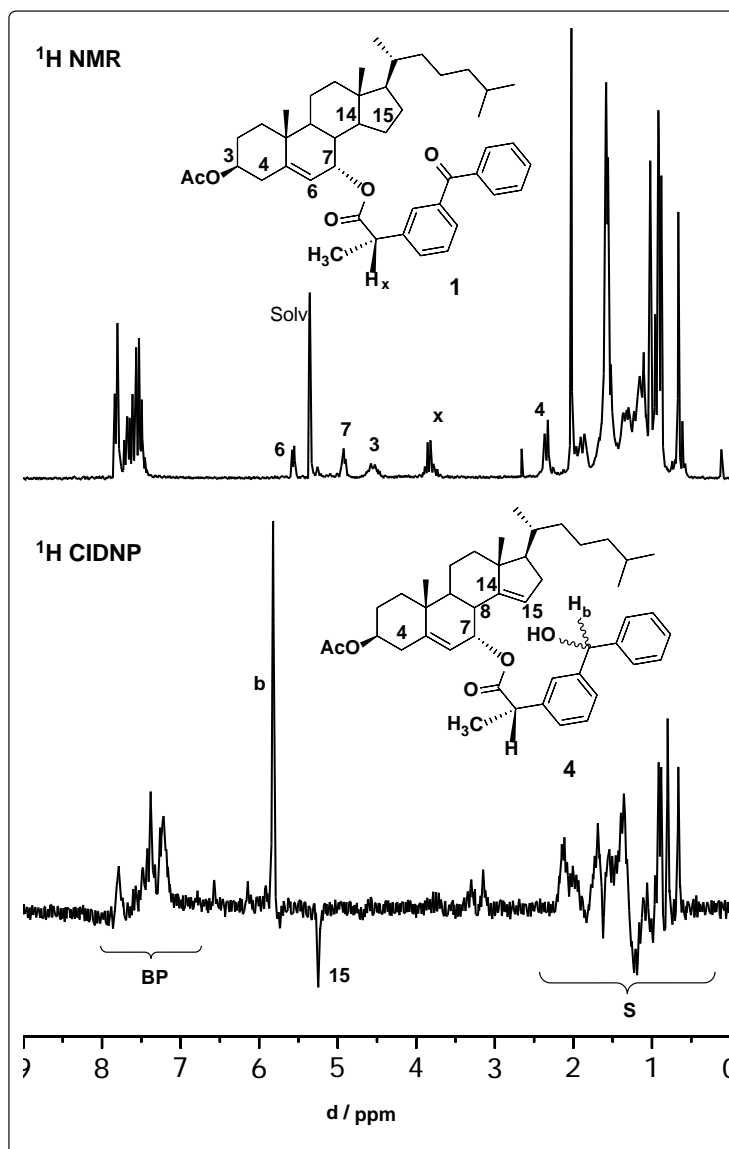
167 Time-resolved photo-CIDNP and quantum mechanical calculations

168 Photo-CIDNP is a powerful NMR-based method to follow reactions based on the initial
169 formation of radical (ion) pairs. These radical pairs react *via* pathways that depend on
170 the electron spin states of the reaction partners.^{24,25} Since nuclear spin states are
171 coupled to the electron spins, this spin-dependent reactivity leads to non-Boltzmann
172 distributions of nuclear spin states. According to the long lifetimes of the non-Boltzmann
173 populated nuclear states the NMR spectra of the products based on the primary radical
174 pair indicate strongly enhanced (up to factor 10^6) emissive ('enhanced emission') or
175 absorptive ('enhanced absorption') signals. The intensity of the NMR signals can be
176 translated into the structure of the intermediate free radicals. Photo-CIDNP can be
177 performed in a time-resolved fashion also revealing kinetic information on free radical
178 reactions.²⁶

179 Here we used TR photo-CIDNP in combination with quantum mechanical calculations to
180 distinguish between reaction pathways and intermediate free radicals formed by **1** after
181 photo-excitation in different solvents.

182 Photo-¹H CIDNP and ¹H NMR spectra of **1** in dichloromethane together with selected
183 signal assignments are shown in Figure 4. The experimental design guarantees the
184 suppression of background (equilibrium) NMR signals in CIDNP spectra, thus only pure
185 CIDNP polarizations with no contamination are observed. The appearance of CIDNP
186 effects *per se* indicates that upon photo-excitation **1** undergoes a free radical reaction
187 that starts with a formation of a correlated radical pair or a biradical that is in concert
188 with the results obtained by LFP. Major polarizations in the CIDNP spectrum of **1** belong
189 to aliphatic protons in the steroid core (S, 0 – 2.5 ppm) and aromatic protons of the
190 benzophenone moiety (BP, 7 – 8 ppm). This denotes that in the intermediate free

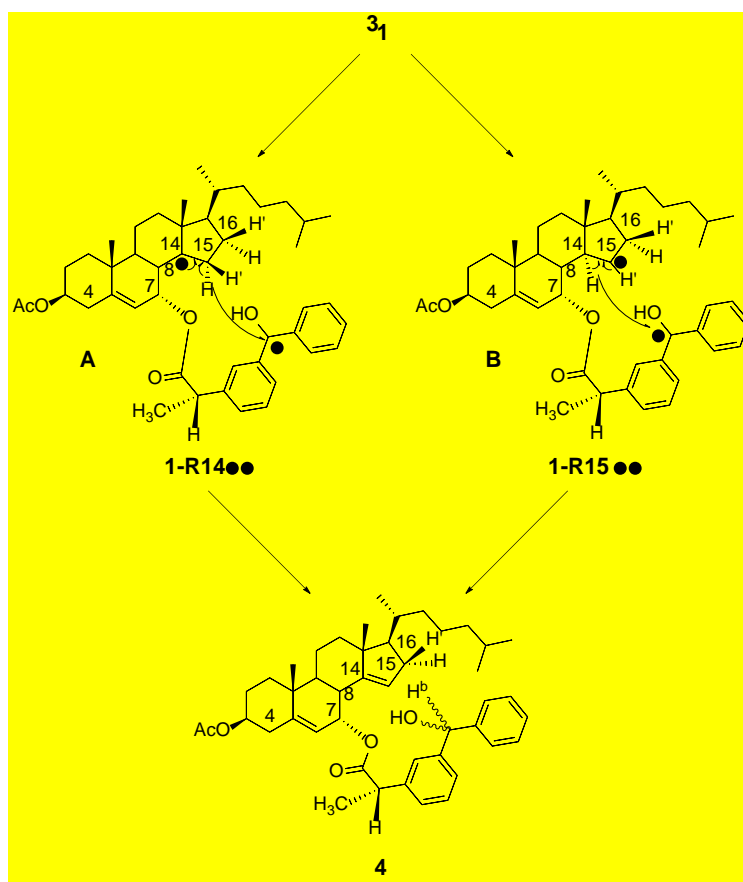
191 radicals both steroid and benzophenone parts carry significant unpaired electron spin
192 density. The NMR transitions of the individual protons **in the S** and BP groups (Figure 4)
193 severely overlap with each other and are difficult to be analyzed further; however, there
194 are two characteristic polarizations in the CIDNP spectrum of **1** that can bring **forth**
195 additional information on the structure of reacting free radicals or biradicals.
196 Polarizations at 5.24 ppm ('enhanced emission') and 5.82 ppm ('enhanced absorption')
197 are unambiguously assigned to protons H15 and Hb in photoproduct **4** (Scheme 2, Figure
198 4). Additionally, two small polarizations are present at 3.1 ppm ('enhanced absorption').
199 They presumably **belong to the proton** at C4 in recombination product **3**.



200

201 **Figure 4.** ^1H NMR (upper trace) and TR-CIDNP (bottom trace) spectra of **1** in dichloromethane- d_2 . CIDNP
 202 spectrum is recorded 2 μs after the laser flash (8 ns, 355 nm)

203 The magnitude of the CIDNP polarizations strongly depends on a hyperfine coupling
 204 constant of corresponding nuclei in free radicals/biradicals where these polarizations
 205 were generated.^{27,28} The very short time-delay between laser flash and observing radio-
 206 frequency pulses allows observation of almost exclusively CIDNP polarizations that are
 207 stored in a cage product formed immediately from the initial radical pair. Thus, the lines
 208 attributed to H15 and H_b in **4** (Figure 4) can be utilized to verify **1-R4••** and **1-R15••**.

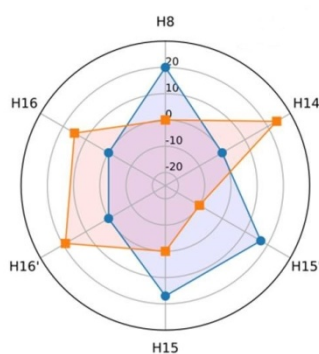


209

210

Scheme 3. Distinct reaction pathways to produce **4**

211 While **3** is the result of the intramolecular hydrogen transfer from C4 carbon of the
 212 steroid moiety, **4** can be formed *via* HA from C15 or C14 (Scheme 3). These reaction
 213 pathways cannot be discriminated by product analysis and LFP. However, intermediate
 214 biradicals **1-R14** and **1-R15** should possess different unpaired spin distributions that
 215 are reflected in different hyperfine couplings of protons in the molecules. This must lead
 216 to different polarizations in CIDNP spectra. We have calculated hyperfine coupling
 217 constants in both possible biradicals **1-R14** and **1-R15** that could be formed upon
 218 HA from C14 and C15 correspondingly. The results for the selected protons are shown
 219 in the radar graph on the Figure 5.



220

221 **Figure 5** Calculated (B3LYP/TZVP) hfc (in Gauss) of selected ^1H nuclei (for numbering, see Scheme 3) in
 222 biradicals **1-R14••** (dots, blue) and **1-R15••** (squares, orange)

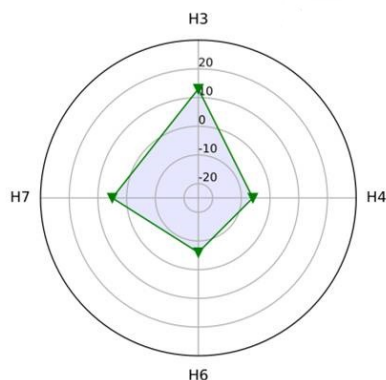
223

224 Thus, it is clear that both biradicals have quite distinct hyperfine patterns. Hyperfine
 225 coupling constants that are plotted in Figure 5 are very different for matching protons
 226 in **1-R14••** and **1-R15••** (H8, H14, H15', H15, H16' and H16). In CIDNP spectrum upon
 227 irradiation of **1** polarizations of H8, H16 and H16' are overlapped with polarizations of
 228 different alkyl protons in parent **1** and/or in **3** and cannot be treated individually. In
 229 contrast, polarizations H15 and Hb (H15 and H15' in **1-R14••**; H14 and H15' in **1-R15••**)
 230 as we **pointed out** before, are clearly distinguishable (Figure 4).

231 There are two possible extreme cases in the photoreaction of **1** where **4** is exclusively
 232 formed *via* pathway **A** or **B** (Scheme 3). In the first case **(path A) the ratio** of the
 233 polarizations of Hb and H15 in **4** will be close to the ratio of **the** corresponding protons
 234 in **1-R14••** ($P_{\text{Hb}}/P_{\text{H15}} \approx \text{hfc}_{\text{H15'}}/\text{hfc}_{\text{H15}} = +17 \text{ Gauss}/+17 \text{ Gauss} = +1$). Moreover, since both
 235 protons have hyperfine coupling **constants** of the same sign, their signals will be
 236 polarized in the same direction. In the second case (path **B**), all the CIDNP effect is
 237 generated in biradical **1-R15••** **and the ratio** of the abovementioned polarizations will

238 be $P_{Hb}/P_{H15} \approx hfc_{H14}/hfc_{H15} = +24 \text{ Gauss}/-10 \text{ Gauss} = -2.4$ with opposite directions of
239 polarization. If **4** is simultaneously produced *via* both pathways the ratio of polarizations
240 will be determined by the superposition of these extreme scenarios. The P_{Hb}/P_{H15}
241 measured from the CIDNP spectrum (Figure 4) is 2.5, which is very close to the prediction
242 for the pathway B. This leads us to the conclusion that in dichloromethane **4** is produced
243 solely *via* hydrogen abstraction from C15 on the timescale of the CIDNP experiment. This
244 contrasts with the results obtained by Breslow and coworkers for other steroidal
245 systems (although lacking the important unsaturation between C5 and C6). He showed
246 the deuteration at position C15 of the steroid moiety, that the primary hydrogen
247 abstraction takes place exclusively from C14. The difference in Breslow's
248 benzophenone-coupled steroids is that linkers attached at the position 3 α of the steroid
249 core were not long enough for the ketone chromophore to reach the hydrogen atom at
250 C15. In **1** the benzophenone moiety can get close to both C14 and C15; this explains HA
251 from C15 but leaves the question as to such a high selectivity towards hydrogen transfer
252 from C15 open. The photoproduct **3** that according to product analysis is formed
253 alongside **4** by the HA from C4 and subsequent intramolecular recombination of
254 biradical **1-R4••**, should also manifest itself in the CIDNP spectrum of **1**. The 'hyperfine
255 signature' of **1-R4••**, where the CIDNP effects were generated, shows that major
256 polarizations in **3** should stem from protons at carbons C3, C4, C6 and C7 of **1-R4••** since
257 they possess the most prominent hyperfine coupling constants according to our
258 quantum mechanical calculations (Figure 6). Unexpectedly, none of them apart from H4
259 (3.1 ppm) gives any significant polarization. This can be rationalized by the longer
260 (relative to **1-R14••** and **1-R15••**) lifetime of **1-R4••** and, possibly, shorter paramagnetic
261 relaxation times of protons H3, H4, H6 and H7 in the biradical. These factors can lead to

262 a vanishing of CIDNP polarizations even before the recombination of the biradical
263 occurs.



264

265 **Figure 6.** Calculated (B3LYP/TZVP) hfcs (in Gauss) of selected ^1H nuclei (for numbering, see Scheme 3) in
266 biradical **1-R4••**(green)

267

268 Dyad **2** did not show any CIDNP effects. This is in full agreement with the product
269 analysis and can be understood in terms of the molecular structure. In **1**, the
270 benzophenone chromophore can adopt a conformation reaching H4, H14 and H15. This
271 is not feasible in **2**, where the benzophenone moiety resides above the steroid skeleton
272 deflecting the ketone oxygen from those protons.

273 According to DFT calculations, the bond dissociation energy (BDE) of the secondary
274 hydrogen at C15 is *ca.* 26 kJ/mol higher than that of C14-H (tertiary hydrogen). If only
275 enthalpic control would rule the reactivity, the hydrogen transfer should exclusively
276 happen from C14. The fact that we exclusively observe abstraction of C15-H reveals
277 entropic/topologic factors being decisive for the hydrogen abstraction.

278 Solvation has a marked effect on the shape of flexible and polar molecules.²⁹ In this
279 respect, we performed (in addition to CD_2Cl_2) ^1H TR-CIDNP experiments in toluene- d_8 ,

280 CDCl₃, and CD₃CN. Table 1 presents the contributions (in %) of HA from C14 vs. C15 taken
281 from the CIDNP intensities determined from product **4**. Whereas in toluene the
282 hydrogen is almost exclusively abstracted from C15 (> 90%), the use of chloroform shifts
283 the ratio between C14-H/C15-H to 1:4 and acetonitrile switches it to 2:3. These
284 observations are in line with a solvent-induced alteration of the preferred conformation
285 of dyad **1**.

286 **Table 1.** Contributions of HA from C14 and C15 into the formation of **4** from **1** in different solvents
287 calculated from TR CIDNP spectra for details, see the Supporting Information).

Solvent	Polarity index ³⁰	HA from C14 (%)	HA from C15 (%)
Toluene-d ₈	2.4	< 10	> 90
CD ₂ Cl ₂	3.1	< 10	> 90
CDCl ₃	4.1	20	80
CD ₃ CN	5.8	40	60

288

289 Conclusion

290 Many biological reactions of cholesterol derivatives are ascribed to reactions in which
291 hydrogen abstraction is involved. Our investigations on dyads **1** and **2** consisting of a **Ch**
292 core and benzophenone show that in addition to the thermodynamically favored H-
293 abstraction at C4, products and radicals based on HA from C15 take place. Such a
294 regioselectivity is not observed in bimolecular reactions of **Ch** and benzophenone in
295 solution. This indicates that a specific orientation of the reactants is crucial for a site-

296 selective reactivity of **Ch**. A confined arrangement of the reactants is very likely to exist
297 in biological membranes containing **Ch**. Our observations are in agreement with clinical
298 studies¹⁶ pointing to the formation of 15 α -hydroxycholestene. Accordingly, our
299 investigation reveals a specific topology being decisive for the reactivity in restricted
300 (anisotropic) biological environments. Finally, selective activation of the strong C15-H
301 bond in the presence of a weaker C7-H allylic bond is of great interest in the C-H
302 functionalization research.

303 **Experimental section**

304 **General**

305 AcetylCh and (S)-KP were commercially available. Other commercial reagents and
306 solvents were used directly without further purification. One- (¹H and ¹³C) and two-
307 dimensional (HSQC and NOESY) NMR spectra were recorded in CDCl₃ as solvent on a
308 Bruker AC-300; NMR chemical shifts are reported in ppm downfield from an internal
309 solvent peak. All reactions were monitored by analytical TLC with silica gel 60 F254
310 revealed with ammonium molybdate reagent. The residues were purified through silica
311 gel 60 (0.063–0.2 mm). Exact mass was obtained by TripleTOF™ 5600 LC/MS/MS System,
312 (AB SCIEX), equipped with an electrospray source. Thus, 7 α -OH-acetylCh or 7 β -OH-
313 acetylCh were synthesized from acetylCh following procedures reported in previous
314 publications. Their ¹H-NMR and ¹³C-NMR signals coincide with those already described
315 in the literature.^{31,32}

316 **Synthesis of dyads 1 and 2**

317 To a solution of (S)-KP (215 mg, 0.84 mmol) in CH₂Cl₂ (5 mL) dicyclohexylcarbodiimide
318 (DCC, 320 mg, 1.54 mmol) was added in small portions, and the mixture was stirred at

319 0°C for 30 min. Then, a solution of 7 α -OH-acetylCh or 7 β -OH-acetylCh (340 mg, 0.77
320 mmol) in CH₂Cl₂ (7 mL) and 4-dimethylaminopyridine (DMAP, 10 mg, 0.08 mmol) was
321 added, and the mixture was kept under stirring overnight at the same temperature. The
322 reaction mixture was then filtered through a pad of Celite®. The resulting filtrate was
323 washed with brine and water, dried over Na₂SO₄ and evaporated. The residue obtained
324 was purified by column chromatography (eluent: dichloromethane-hexane-
325 dichloromethane acetate 90:5:5 v/v/v) to give dyad **1** (355 mg, 0.52 mmol, 68%) and
326 dyad **2** (405 mg, 0.59 mmol, 77 %).

327 **(3S,7S,10R,13R,17R)-3-acetoxy-10,13-dimethyl-17-((R)-6-methylheptan-2-yl)2,3,4,7,8,**
328 **9,10,11,12,13,14,15,16,17-tetradecahydro-1H-cyclopenta[α]phenanthren-7-yl (2S)-2-**
329 **(3-benzoylphenyl)propanoate (1).** ¹H-NMR (300 MHz, CDCl₃) δ = 7.35-7.74 (m, 9H, ArH),
330 5.48 (m, 1H, C6-H), 4.84 (m, 1H; C7-H), 4.48 (m, 1 H; C3-H), 3.74 (q, J = 7.2 Hz, 1H; CH₃-
331 CH-CO), 2.25 (m, 2H; C4-H₂), 1.96 (s, 3H; CH₃), 0.98-1.94 (complex signal, 24H), 1.49 (d,
332 J = 7.2 Hz, 3H; CH₃), 0.91 (s, 3H; CH₃), 0.82 (d, J = 6.6 Hz, 3H; CH₃), 0.80 (d, J = 6.6 Hz, 3H;
333 CH₃), 0.79 (d, J = 6.6 Hz, 3H; CH₃), 0.54 (s, 3H; CH₃); ¹³C{¹H} (75 MHz, CDCl₃) δ = 196.3,
334 173.4, 170.3, 147.1, 140.8, 137.6, 132.3, 131.7, 130.0, 129.4, 129.1, 128.3, 120.3, 73.2,
335 68.9, 55.9, 49.1, 45.9, 43.2, 42.1, 39.5, 39.1, 37.8, 37.3, 36.6, 36.1, 35.9, 35.8, 28.0, 27.4,
336 24.0, 22.8, 22.5, 21.3, 20.7, 18.7, 18.1, 17.9, 11.4. HRMS (EI): m/z calcd for C₄₅H₆₁O₅
337 (M+H)⁺: 681.4514; found: 681.4492.

338 **(3S,7R,10R,13R,17R)-3-acetoxy-10,13-dimethyl-17-((R)-6-methylheptan-2yl)2,3,4,7,8,**
339 **9,10,11,12,13,14,15,16,17-tetradecahydro-1H-cyclopenta[α]phenanthren-7-yl (2S)-2-**
340 **(3-benzoylphenyl)propanoate (2).** ¹H-NMR (300 MHz, CDCl₃) δ = 7.18-7.82 (m, 9H; ArH);
341 5.24 (m, 1H; C6-H), 4.98 (m, 1H; C7-H), 4.61 (m, 1H; C3-H), 3.74 (q, J = 7.2 Hz, 1H; CH₃-

342 CH-CO), 0.67-2.37 (complex signal, 29H), 2.05 (s, 3H; CH₃), 1.55 (d, *J* = 7.2 Hz, 3H; CH₃),
343 1.09 (s, 3H; CH₃), 0.88 (d, *J* = 6.6 Hz, 3H; CH₃), 0.87 (d, *J* = 6.3 Hz, 3H; CH₃), 0.59 (s, 3H;
344 CH₃); ¹³C{¹H} (75 MHz, CDCl₃) δ = 196.4, 173.8, 170.3, 144.5, 140.6, 137.7, 137.6, 132.4,
345 131.8, 130.0, 129.7, 129.0, 128.4, 128.3, 122.0, 73.2, 55.4, 53.4, 48.2, 45.7, 42.7, 39.5,
346 39.3, 38.2, 37.6, 36.5, 36.4, 36.3, 36.1, 35.7, 31.2, 30.9, 29.7, 28.0, 27.6, 25.1, 23.8, 22.8,
347 22.5, 21.3, 21.1, 18.9, 18.6, 18.2, 11.7. HRMS (EI): *m/z* calcd for C₄₅H₆₁O₅ (M+H)⁺:
348 681.4514; found: 681.4495.

349 **Steady-state photolysis of dyads 1 and 2**

350 Deaerated dichloromethane (40 mL) solutions of **1** or **2** (100 mg, 0.15 mmol) were
351 irradiated for 8 h through Pyrex with a 400 W medium pressure mercury lamp. After
352 that, the reaction mixtures were concentrated under reduced pressure, and the
353 photomixtures were submitted to silica gel column chromatography, using
354 hexane/dichloromethane/ethyl acetate (85:10:5 v/v/v) as eluent, affording the
355 photoproducts **3** (23 %) and **4** (diastereomeric mixture, 25 %); the rest was mixture of
356 several minor unidentified products, together with polymeric material. Moreover, to
357 determine the photoreduction quantum yield of dyad **1** in dichloromethane, (S)-KP-
358 3α-Ch was used as actinometer, with a quantum yield of 0.47.²² For this purpose,
359 solutions of **1** and the actinometer were photolyzed under deaerated conditions using
360 a multilamp photoreactor model LZC-4 (Luzchem, Canada) equipped with 8 lamps (λ_{max}
361 = 350 nm, Gaussian distribution) and monitored by UV-spectrophotometry following the
362 decrease in the absorption at 254 nm. Thus, the quantum yield was calculated from the
363 slope of the plot absorbance at 254 nm versus irradiation time.

364 **(3R,3aR,5aS,6R,9S,17S,20S)-3[(1R)-1,5-dimethylhexyl]1,2,3,3a,4,5,5a,6,7,8,9,10,11,**
365 **20,20a,21-hexadecahydro-11-hydroxy-7a,6,17trimethyl-11-phenyl-20,6,10-etheno-**
366 **12,16-methenoindeno[5,4f]oxacycloheptadecin-18(17H)-one (3).** ¹H-NMR (300 MHz,
367 CDCl₃) δ = 7.71 (m, 1H; ArH), 7.22-7.39 (m, 6H; ArH), 7.12 (m, 1H; ArH), 6.51 (s, 1H; ArH),
368 5.47 (d, *J* = 5.1 Hz, 1H; C6-H), 4.53 (m, 1H; C7-H), 4.47 (m, 1H; C3-H), 3.70 (q, *J* = 7.5 Hz,
369 1H; CH₃-CH-CO), 3.05 (m, 1H; C4-H), 2.22 (m, 2H; C2-H₂), 1.95 (s, 3H; CH₃), 0.42-1.90
370 (complex signal, 22H), 1.46 (d, *J* = 7.5 Hz, 3H; CH₃), 1.07 (d, *J* = 7.2 Hz, 3H; CH₃), 0.84 (s,
371 3H; CH₃), 0.81 (d, *J* = 6.6 Hz, 6H; 2 × CH₃), 0.60 (s, 3H; CH₃), -0.45 (m, 1H; CH); ¹³C{¹H} (75
372 MHz, CDCl₃) δ = 175.6, 170.4, 148.1, 146.9, 143.2, 138.7, 130.0, 129.8, 128.4, 128.3,
373 128.1, 127.8, 126.8, 126.4, 122.7, 120.4, 82.1, 73.2, 69.1, 55.9, 45.7, 44.0, 43.9, 43.7,
374 42.9, 39.4, 38.4, 37.6, 37.2, 36.4, 36.3, 35.3, 32.5, 30.8, 28.1, 27.4, 26.2, 22.8, 22.7, 21.3,
375 20.6, 20.0, 17.9, 14.3, 14.2. HRMS (EI): *m/z* calcd for C₄₅H₆₁O₅ (M+H)⁺: 681.4514; found:
376 681.4518.

377 **(3S,7R,10R,13R,17R)-3-acetoxy-10,13-dimethyl-17-((R)-6-methylheptan-2-yl)-2,3,4,7,**
378 **8,9,10,11,12,13,16,17-dodecahydro-1H-cyclopenta[a]phenanthren-7-yl(2S)-2-(3-**
379 **(hydroxy(phenyl)methyl)phenyl)propanoate (4, diastereomeric mixture).** ¹H-NMR
380 (300 MHz, CDCl₃) δ = 7.08 – 7.32 (m, 9H; ArH), 5.73 (m, 1H; Ph-CH-OH), 5.47 (m, 1H; C6-
381 H), 5.12 (m, 1H; C15-H), 4.90 (m, 1H; C7-H), 4.36 (m, 1H; C3-H), 3.64 (q, *J* = 7.2 Hz, 1H;
382 CH₃-CH-CO), 2.94 (m, 1H; C4-H), 2.82 (m, 1H; C4-H), 0.56 – 2.28 (complex signal, 35H),
383 1.95 (d, *J* = 1.8 Hz, 3H; CH₃), 0.79 (d, *J* = 6.6 Hz, 3H; CH₃), 0.78 (d, *J* = 6.6 Hz, 3H; CH₃),
384 0.67 (s, 3H; CH₃); ¹³C{¹H} (75 MHz, CDCl₃) δ = 174.0, 173.9, 170.8, 170.7, 160.5, 160.4,
385 146.9, 146.8, 144.4, 144.3, 144.1, 140.7, 139.3, 128.6, 128.5, 128.4, 128.3, 127.4, 127.3,
386 127.0, 126.6, 126.5, 125.6, 125.5, 125.2, 125.1, 120.6, 120.5, 120.4, 120.3, 114.1, 76.0,

387 75.9, 73.5, 73.4, 68.9, 68.8, 50.3, 50.2, 46.9, 45.6, 45.5, 43.5, 43.4, 39.2, 37.8, 37.5, 36.8,
388 36.6, 36.5, 34.7, 34.5, 32.2, 31.9, 30.9, 29.7, 27.9, 27.5, 27.4, 25.3, 22.7, 22.6, 21.9, 21.8,
389 21.4, 20.5, 18.1, 17.7, 17.5, 15.8, 14.1. HRMS (EI): m/z calcd for $C_{45}H_{61}O_5$ (M+H)⁺:
390 681.4514; found: 681.4507.

391 **Laser flash photolysis measurements**

392 A pulsed Nd:YAG laser was used for excitation at 355 nm. The single pulse was ~10 ns
393 duration and the energy ranging from 10 to 1 mJ pulse⁻¹. The LFP system consisted of the
394 pulsed laser, the Xe lamp, a monochromator and a photomultiplier made up of a tube,
395 housing and power supply. The output signal from the oscilloscope was transferred to a
396 personal computer. All experiments were performed at room temperature under
397 anaerobic conditions. The samples were dissolved in dichloromethane to have an
398 absorbance *ca.* 0.30 at 355 nm.

399 **CIDNP and quantum mechanical calculations of hyperfine coupling constants**

400 ¹H CIDNP spectra were recorded on a 200 MHz Bruker AVANCE DPX spectrometer.
401 Irradiation was carried out by using a frequency-tripled Quantel Nd:YAG Brilliant B laser
402 (10 Hz, 355 nm, *ca.* 90 mJ per pulse, pulse width *ca.* 8 ns). The following pulse sequence
403 was used: presaturation (waltz16) – laser flash – RF detection pulse (2 μs) – free
404 induction decay. Dark spectra (background) - the same sequence without the laser flash
405 - were always recorded to assure the effective suppression of background NMR signals.
406 The concentrations of **1** and **2** were 0.01 M. To exclude oxygen, samples were bubbled
407 with Argon for 5 minutes prior to experiments. Hyperfine coupling constants of free
408 radicals were calculated using the Gaussian 09³³ package. All calculations (geometry

409 optimizations and single-point calculations) were conducted at the B3LYP^{34,35} level of
410 theory with the TZVP³⁶ basis set.

411 **Calculation of the contributions of 1-R14•• and 1-R15•• biradicals into CIDNP**
412 **polarizations of H15 and Hb protons.**

413 Polarizations of Hb (P_{Hb}) and H15 (P_{H15}) can be measured directly from the spectrum and
414 their ration is:

$$415 \quad \frac{P_{Hb}}{P_{H15}} = -2.4 \quad (1)$$

416 Polarization of Hb is constructed from contributions of **1-R14••** and **1-R15••** which are
417 proportional to hyperfine coupling constants of corresponding protons in those
418 biradicals and:

$$419 \quad P_{Hb} = C \times a_{H14}^{R15} + (1 - C) \times a_{H15}^{R14} \quad (2)$$

420 Where a_{H14}^{R15} and a_{H15}^{R14} are hiperfine coupling protons H14 and H15 in biradicals **1-R15••**
421 and **1-R14••** correspondingly. Analogously the polarization of H15 is represented:

$$422 \quad P_{H15} = C \times a_{H15}^{R15} + (1 - C) \times a_{H15}^{R14}, \quad (3)$$

423 The system of equations 1-3 can be solved with respect to proportionality constant C
424 which gives us contributions of 2 different biradicals into CIDNP polarizations.

425 **Associated content**

426 **Supporting Information**

427 **The Supporting Information is available free of charge on the...**

428 **Scheme of the synthesis of dyads 1 and 2 (Scheme S1); ¹H and ¹³C-NMR spectra of 7-**

429 **oxo-acetylCh; ¹H and ¹³C-NMR spectra of 7α-OH-acetylCh; ¹H and ¹³C-NMR spectra of**

430 **7 β -OH-acetylCh**; ¹H, ¹³C-NMR and DEPT spectra of dyad **1**; ¹H, ¹³C-NMR and DEPT spectra
431 of dyad **2**; ¹H, ¹³C-NMR, DEPT, HSQC and NOESY spectra of photoproduct **3**; ¹H, ¹³C-NMR,
432 DEPT, HSQC and NOESY spectra of photoproduct **4**; calculations B3LYP/TZVP optimized
433 model for dyad **1** and **2**.

434 Acknowledgements

435 This work was supported by the Carlos III Institute of Health (Grants: PI16/01877,
436 “Miguel Servet fellowship” CPII16/00052 to I.A), and by the Generalitat Valenciana
437 (Prometeo 2017/075). We would like to thank Dr. Fedora Grande for sending an
438 exchange student (M.B) DN and GG thank NAWI Graz for support.

439 References

- 440 1 Zerbinati, C., Iuliano L. Cholesterol and related sterols autoxidation. *Free Radic. Biol. Med.* **2017**,
441 *111*, 151–155.
- 442 2 Schroepfer, G. J. Oxysterols: modulators of cholesterol metabolism and other processes. *Physiol.*
443 *Rev.* **2000**, *80*, 361–554.
- 444 3 Girotti, A. W., Korytowski, W. Cholesterol hydroperoxide generation, translocation, and reductive
445 turnover in biological systems. *Cell Biochem. Biophys.* **2017**, *75*, 413–419.
- 446 4 Poli, G., Biasi, F., Leonarduzzi, G. Oxysterols in the pathogenesis of major chronic diseases. *Redox*
447 *Biol.* **2013**, *1*, 125–130.
- 448 5 Buttari, B., Segoni, L., Profumo, E., D’Arcangelo, D., Rossi, S., Facchiano, F., Businaro, R., Iuliano,
449 L., Rigano, R. 7-oxo-cholesterol potentiates pro-inflammatory signaling in human M1 and M2
450 macrophages. *Biochem. Pharmacol.* **2013**, *86*, 130–137.
- 451 6 Scheinost, J. C., Wang, H., Boldt, G. E., Offer, J., Wentworth, P. Cholesterol seco-sterol-induced
452 aggregation of methylated amyloid-beta peptides--insights into aldehyde-initiated fibrillization of

453 amyloid-beta. *Angew. Chemie Int. Ed.* **2008**, *47*, 3919–3922.

454 7 Shahidi, F., Zhong, Y. Lipid oxidation and improving the oxidative stability. *Chem. Soc. Rev.* **2010**,
455 39, 4067–4079.

456 8 Zielinski, Z. A. M., Pratt, D.A. Lipid peroxidation: kinetics, mechanisms, and products. *J. Org. Chem.*
457 **2017**, *82*, 2817–2825.

458 9 Sarzi-Puttini, P., Atzeni, F., Lanata, L., Bagnasco, M. Efficacy of ketoprofen vs. ibuprofen and
459 diclofenac: a systematic review of the literature and meta-analysis. *Clin. Exp. Rheumatol.* **2013**,
460 31, 731–738.

461 10 Bignon, E., Marazzi, M., Besancenot, V., Gattuso, H., Drouot, G., Morell, C., Eriksson, L. A.,
462 Grandemange, S., Dumont, E., Monar, A. Ibuprofen and ketoprofen potentiate UVA-induced cell
463 death by a photosensitization process. *Sci. Rep.* **2017**, *7*, 8885.

464 11 Bagheri, H., Lhiaubet, V., Montastruc, J. L., Chouini-Lalanne, N. Photosensitivity to ketoprofen:
465 mechanism and pharmacoepidemiological data. *Drug Saf.* **2000**, *22*, 339–349.

466 12 Breslow, R. Biomimetic control of chemical selectivity. *Acc. Chem. Res.* **1980**, *13*, 170–177.

467 13 Breslow, R., Baldwin, S., Flechtner, T., Kalicky, P., Liu, S., Washburn, W. Remote oxidation of
468 steroids by photolysis of attached benzophenone groups. *J. Am. Chem. Soc.* **1973**, *95*, 3251–3262.

469 14 Zielinski, Z. A. M., Pratt, D. A. Cholesterol autoxidation revisited: debunking the dogma associated
470 with the most vilified of lipids *J. Am. Chem. Soc.* **2016**, *138*, 6932–6935.

471 15 Garrec, J., Monari A., Assfeld, X., Mir, L. M., Tarek, M. Lipid peroxidation in membranes: the
472 peroxy radical does not “float”. *J. Phys. Chem. Lett.* **2014**, *5*, 1653–1658.

473 16 Farez, M., Quintana, F. J., Gandhi, R., Izquierdo, G., Lucas M., Weiner, H. L. Toll-like receptor 2 and
474 poly(ADP-ribose) polymerase 1 promote central nervous system neuroinflammation in
475 progressive EAE. *Nat. Immunol.* **2009**, *10*, 958–964.

476 17 Björkhem, I., Lövgren-Sandblom, A., Piehl, F., Khademi, M., Pettersson, H., Leoni, V., Olsson, T.,
477 Diczfalusy, U. High levels of 15-oxygenated steroids in circulation of patients with multiple
478 sclerosis: fact or fiction? *J. Lipid Res.* **2011**, *52*, 170–174.

479 18 Davies, H., Morton, D. Collective approach to advancing C–H functionalization. *ACS Cent. Sci.*
480 **2017**, *3*, 936–943.

481 19 Gutekunst, W. R., Baran, P. Applications of C–H functionalization logic to cyclobutane synthesis.

482 *J. Org. Chem.* **2014**, *79*, 2430-2452.

483 20 Neshchadin, D., Palumbo, F., Sinicropi, M. S., Andreu, I., Gescheidt, G., Miranda, M. A. Topological
484 control in radical reactions of cholesterol in model dyads. *Chem. Sci.* **2013**, *4*, 1608-1614.

485 21 Andreu, I., Morera, I. M., Boscá, F., Sanchez, L., Camps, P., Miranda, M. A. Cholesterol–diaryl
486 ketone stereoisomeric dyads as models for “clean” type I and type II photooxygenation
487 mechanisms. *Org. Biomol. Chem.* **2008**, *6*, 860–867.

488 22 Andreu, I., Palumbo, F., Tilocca, F., Morera, I. M., Bosca, F., Miranda, M. A. Solvent effects in
489 hydrogen abstraction from cholesterol by benzophenone triplet excited state. *Org. Lett.* **2011**, *13*,
490 4096-4099.

491 23 Bosca, F., Andreu, I., Morera, I. M., Samadi, A., Miranda, M. A. Chiral discrimination in the
492 intramolecular abstraction of allylic hydrogens by benzophenone triplets. *Chem. Commun.* **2003**,
493 1592-1593.

494 24 Kaptein, R., Oosterhoff, L. J. Chemically induced dynamic nuclear polarization III (anomalous
495 multiplets of radical coupling and disproportionation products). *Chem. Phys. Lett.* **1969**, *4*, 214–
496 216.

497 25 Closs, G. L. Mechanism explaining nuclear spin polarizations in radical combination reactions. *J.*
498 *Am. Chem. Soc.* **1969**, *91*, 4552–4554.

499 26 Vollenweider, J. K., Fischer, H., Hennig, J., Leuschner, R. Time-resolved CIDNP in laser flash
500 photolysis of aliphatic ketones. A quantitative analysis. *Chem. Phys.* **1985**, *97*, 217–234.

501 27 Neshchadin, D., Levinn, R., Gescheidt, G., Batchelor, S.N. Probing the antioxidant activity of
502 polyphenols by CIDNP: from model compounds to green tea and red wine. *Chem. - A Eur. J.* **2010**,
503 *16*, 7008–7016.

504 28 Yurkovskaya, A., Morozova, O., Gescheidt, G. *Encycl. Radicals Chem. Biol. Mater.* (John Wiley &
505 Sons, Ltd, Chichester, UK, **2012**)

506 29 Reichardt, C. *Solvents and Solvent Effects in Organic Chemistry* (Wiley-VCH, **2003**).

507 30 Kier, L. B. Quantitation of solvent polarity based on molecular structure. *J. Pharm. Sci.* **1981**, *70*,
508 930–933.

509 31 Poza, J., Rega, M., Paz, V., Alonso, B., Rodríguez, J., Salvador, N., Fernández, A., Jiménez, C.
510 Synthesis and evaluation of new 6-hydroximinosteroid analogs as cytotoxic agents. *Bioorg. Med.*
511 *Chem.* **2007**, *15*, 4722-4740.

512 32 Poza, J. J., Jiménez, C., Rodríguez, J. J-Based Analysis and DFT–NMR Assignments of Natural
513 Complex Molecules: Application to 3 β ,7-Dihydroxy-5,6-epoxycholestanes. *Eur. J. Org. Chem.*
514 **2008**, *23*, 3960-3969.

515 33 Frisch, M. J., Trucks, G. W., Schlegel, H. B., Scuseria, G. E., Robb, M. A., Cheeseman, J. R., Scalmani,
516 G., Barone, V., Mennucci, B., Petersson, G. A. et al. *Gaussian 09, Revision D.01*. Gaussian, Inc.:
517 Wallingford, CT, USA, **2009**.

518 34 Stephens, P. J., Devlin, F. J., Chabalowski, C. F., Frisch, M. J. *J. Phys. Chem.* **1994**, *98*, 11623–11627.

519 35 Becke, A. D. *J. Chem. Phys.* **1993**, *98*, 5648–5652.

520 36 Schäfer, A., Horn, H., Ahlrichs, R. *J. Chem. Phys.* **1992**, *97*, 2571–2577.

521